FOURIER TRANSFORM INFRARED BROADBAND SPECTROSCOPY OF THE GAS PHASE OF HF AND CO MIXTURES

A.S. SIZHUK

Physics Department, Texas A&M University
(College Station, Texas 77843-4242, USA; e-mail: cannabiss@mail.univ.kiev.ua)

UDC 539.1

The gas phase spectra of hydrogen fluoride (HF) and carbon oxide (CO) mixtures are investigated using the Fourier transform infrared (FTIR) broadband spectroscopy technique for the region from 3838 to 3854 cm^{-1}. The OC–HF complex bands, that can correspond to the excited intermolecular (complex) stretching and bending, are observed for the partial mixture pressures of 20 Torr of HF and 30 Torr of CO and higher. The corresponding hot bands of the second harmonic for the bending mode are observed at the total pressure of 100 Torr at -15 degree Celsius (corresponding to 26 Torr of HF and about 90 Torr of CO at room temperature). The observed hot bands are assigned with the help of the fitted spectra for a slightly non-rigid linear molecule. The fitting for the model linear molecule with the experimental data produced the following parameters for the excited states v_1, $v_1 + v_5^1$ and $v_1 + v_3$: $v_1 = 3844.030345$ cm^{-1} with $B(v_1) = 0.104181$ cm^{-1} and $D(v_1) = 3.447151 \times 10^{-7}$ cm^{-1}; $v_1 + v_5^1 = 3931.406563$ cm^{-1} with $B(v_1 + v_5^1) = 0.105090$ cm^{-1} and $D(v_1 + v_5^1) = 3.31263 \times 10^{-7}$ cm^{-1}; $v_1 + v_3 = 3960.722190$ cm^{-1} with $B(v_1 + v_3) = 0.102764$ cm^{-1} and $D(v_1 + v_3) = 3.059578 \times 10^{-7}$ cm^{-1}, respectively.

1. Introduction

OC–HF complex was the subject of a quite large number of both experimental and later theoretical investigations. A significant number of reviews and books have also been published, by detailing the application of experimental methods, particularly those that are spectroscopic (see, for example, [1–5]), as well as the development of appropriate computational methods [6–14]. Most of the experimental and theoretical investigations of OC–HF (CO–HF) complexes were carried out under isolated conditions (gas mixtures rarefied to a few Torrs at temperatures below -30 Celsius or supersonic jet expansions). The detailed theoretical studies are still primarily concerned with simple isolated complexes [15], [16]. The pairwise interactions are particularly important for the accurate prediction of properties of the intermolecular interaction, such as equilibrium and vibrational state-specific geometries, dissociation energies, transition frequencies, *etc.* Such an approach facilitates the determination of the fundamental properties of simpler prototypical systems without emphasizing the process of creation of complexes that can involve three-body interactions or an additional, "out of bound state", interaction characteristic.

The OC–HF complex was first observed experimentally, using pulsed supersonic jet Fourier transform microwave spectroscopy [1, 17]. These studies indicated that the equilibrium geometry was linear with the atoms configured in the non-linear ground configuration as in Fig. 1. In addition, electric and magnetic properties of OC–HF have also been studied in [18, 19]. We tried to achieve some progress in characterizing the properties of two small covalent molecules quite close distanced. This has been particularly done, by using high resolution spectroscopic techniques, especially in the gas phase. Some important spectroscopic characteristics, like the dependence of a line intensity on the molecular densities, can be found, by using Fourier transform infrared (FTIR) technique. Certain features in the dependence of complex band intensities on molecular densities can help to understand more deeper the nature of the weak bonding. We will discuss it in what follows.

OC–HF dimer is a weaker member of the group with medium-strength hydrogen-bonded interaction [12]. An

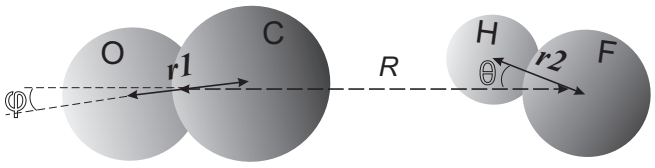

Fig. 1. Geometry of the complex OC-HF in its ground states. The sketch is based on data provided in [1], [20]: Planar OC-HF complex ground state geometry: $R = 365$ pm is the distance between the centers of masses of OC and HF monomers; $\varphi = 14°$, $\theta = 22°$. Approximately, in a monomer OC, the distance between atoms O and C is $r1 = 113$ pm; in a HF monomer, the distance between atoms H and F is $r2 = 92$ pms. The relative radius of each atom in the monomers above is taken as the covalent radius from the table of covalent radii in [21]. The angles φ and θ usually correspond in the literature to the angles θ_1 and $\pi - \theta_2$, respectively

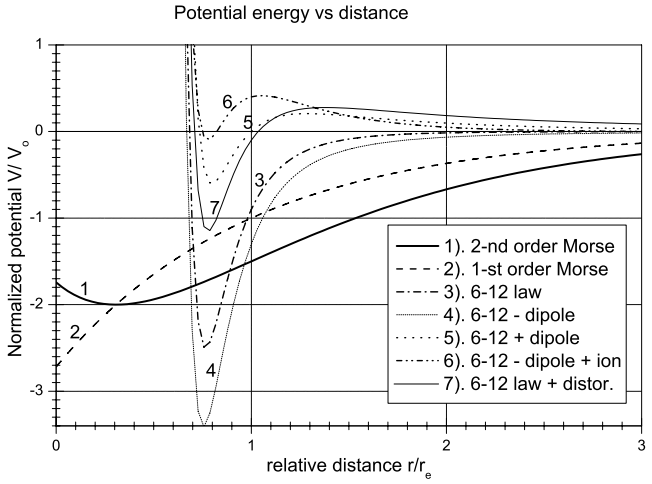

Fig. 2. Relative potential energy vs the relative distance. Here, *1* corresponds to the dependence $V/V_0 = -(1.5 - (1 - \exp(-(x - 1))) - 0.5(1 - \exp(-(x - 1)))^2)$; *2* corresponds to $V/V_0 = -(1 - (1 - \exp(-(x - 1))))$; *3* is $V/V_0 = -1/x^6 + 0.1/x^{12}$; *4* is $V/V_0 = -1/x^6 + 0.1/x^{12} - 0.4/x^3$; *5* is $V/V_0 = -1/x^6 + 0.1/x^{12} + 0.9/x^3$; and *6* is $V/V_0 = -2/x^6 + 0.1/x^{12} - 1/x^3 + 3.3/x^4$; *7* is $V/V_0 = -1/x^6 + 0.1/x^{12} + 0.8/x^2$ and includes the rotationally induced distortion potential in addition to the 12–6 dependence, where V_0 denotes some equilibrium (ground state) potential energy, and $x = r/r_e$ denotes the distance between the centers of masses of monomers relative to some equilibrium quantity r_e

isolated OC–HF dimer is relatively well characterized by high-resolution spectroscopy. It was initially identified using pulsed-nozzle Fourier transform microwave spectroscopy and was one of the first complexes investigated by ro-vibrationally resolved gas phase infrared spectroscopy [1, 22, 4]. Based on ground state microwave spectroscopy, OC–HF was determined to be linear in its equilibrium geometry with the monomers bonded through the carbon atom. In the ground vibrational state, it is a very nearly prolate asymmetric top, in which only $K = 0$ transitions are observed. The complex has since been a subject of the extensive further spectroscopic characterization. Such analysis included, most importantly, a precise experimentally determined dissociation energy, a study of the state-specific vibrational predissociation and a simulated analysis of the third harmonic of the HF vibration at 10894.46(1) cm^{-1} that is significantly greater than the ground state dissociation energy determined to be 732(2) cm^{-1} [23, 24]. It is also a system that has been a subject of the extensive previous computational study as a prototypical hydrogen-bonded dimer involving first row atoms [25, 39]. The approaches developed in [40] for OC–HF are based on adaptations of the previously developed potential compound-model (PCM) and the compound-model morphing (CMM) techniques [41, 42]. We use the obtained predictions to compare with our experimental results.

The characteristic frequencies of spectra obtained in this work are compared with the theoretically predicted by the compound-model "morphing" with radial shifting (CMM-RS) approach [40] and those obtained by the supersonic beam and color center laser spectrometer [5]. The CMM-RS methodology presented in work [40], based on *ab initio* potential grids, uses the reproducing kernel Hilbert space [43] fitting functions, giving raise in the dipole-dipole interaction at quite long distances, to interpolate the radial coordinates of the six-dimensional potential for OC–HF. The experimental data, used to "morph" the intermolecular potential energy surface of OC–HF in [40], include 24 points from [1–5] (such like rotational constants B_{ground}, $B(v_1)$, $B(v_1+v_5^1)$; frequencies of the band centers v_1, $v_1 + v_5^1 - v_5^1$, $v_1 + v_3 - v_3$, *etc.*).

The corresponding potential surface [40] does not possess a local maximum above the "zero" level with respect to the distance between the monomers, therefore, leaving the open question about the processes that "make the complex happened". Hence, if we consider the complex structure in Fig. 1 with the attractive dipole-dipole interaction between the monomers, such kind of hydrogen bonding potential should have significant enough contributions from the rotationally induced distortion energy and/or the item of ionic interaction as in examples *6* and *7* in Fig. 2, where some possible potential curves $V(r)$ (r denotes the distance between the centers of masses of monomers) are depicted.

Respectively, our paper consists of the two main parts: experimental observations and the discussion of the obtained results.

2. Experimental Results

The values of the ν_1, ν_2, and ν_4^1 modes of vibrational frequencies were initially determined to be 3789.3(3) cm^{-1}, 2162.4(3) cm^{-1} and 389.5(5) cm^{-1}, using infrared spectra in solid argon matrices [44]. Analysis of the intramolecular bands ν_1 and ν_2 located at 3844.0294(50) cm^{-1} and 2167.69904(11) cm^{-1} under isolated equilibrium gas phase and slit jet expansion conditions were reported using a single-frequency mode hop color center laser [22] and diode laser spectroscopy [4], respectively. A reinvestigation of the sub-Doppler resolution infrared spectrum of the ν_1 intramolecular band [45] provided a precise evaluation of the excited state life-

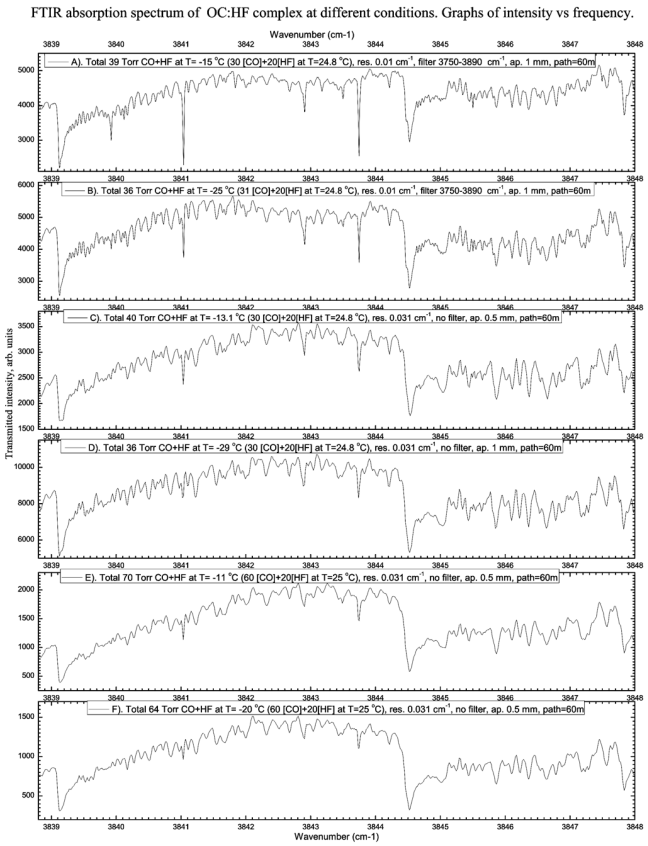

Fig. 3. Absorption spectrum of OC–HF at different temperatures and pressures. *A–D* for the initial pressures at room temperature 30 ± 1 Torr of CO and 20 ± 1 Torr of HF; *E–F* for the initial pressures at room temperature 60 ± 1 Torr of CO and 20 ± 1 Torr of HF

time, namely 0.9(1) ns. A further investigation recorded the hot bands associated with the ν_1 intramolecular band [5] and an estimation of the ν_5^1 vibrational frequency to be 80.(12) cm^{-1}. In this work, the gas phase spectra of CO and HF mixtures were investigated using the FTIR spectrometer technique for the region from 3838 to 3954 cm^{-1}. The OC–HF complex bands that can correspond to the excited intermolecular (complex) stretching and bending were observed for the total mixture density corresponding to 100 Torr at -15 degree Celsius (approximately corresponding to 26 Torr of HF and 90 Torr of CO at room temperature). The observed bands shown in Figs. 3–7 (Fig. 4 for the pure HF component is given for the comparison) can be assigned as theoretically predicted by the compound-model "morphing" approach in [40]: v_1 H-F stretching fundamental in the OC–HF complex is 3844.02776 cm^{-1}; theoretical $v_1 + v_5^1 - v_5^1$ hot band is at 3849.4416 cm^{-1}; theoretical $v_1 + v_3 - v_3$ hot band is at 3851.972 cm^{-1}; where

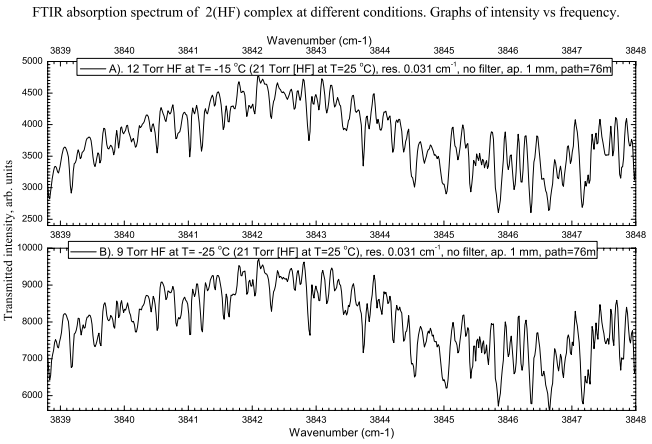

Fig. 4. Absorption spectrum of HF (mainly, 2(HF) dimer) at different temperatures. *A–B* for the initial pressures at room temperature 21 ± 1 Torr of HF

the bending $v_5^1 = 81.97997$ cm^{-1}; rotational constant in the ground state $B(GS) = 0.10221$ cm^{-1}; in the excited state v_5^1: $B(v_5^1) = 0.10304$ cm^{-1}; in the excited state v_3: $B(v_3) = 0.09958$ cm^{-1}; in the excited state v_1: $B(v_1) = 0.10426$ cm^{-1}; in the excited state $v_1 + v_5^1$: $B(v_1 + v_5^1) = 0.10510$ cm^{-1}; in the excited state $v_1 + v_3$: $B(v_1 + v_3) = 0.10178$ cm^{-1}. In the sense of the provided possible assignment, we can see the corresponding *P*-heads at approximately 3839.12 cm^{-1} in Fig. 7 for the v_1 H-F stretching fundamental in the OC–HF, 3844.5 cm^{-1} for $v_1 + v_5^1 - v_5^1$, and 3847.85 cm^{-1} for $v_1 + v_3 - v_3$, with new unassigned 3850.07 cm^{-1}, and 3852.05 cm^{-1} lines (the heads of bands).

Our experimental data were obtained under certain conditions of the gas phase of the mixture (temperatures, pressures, resolutions, *etc.*), using a BOMEM DA8 Fourier transform spectrometer system with multiple-path White cell (a stainless steel chamber about 2 m in length and 0.18 m in diameter) and a cryogenic cooling system, with a detector InSb (1800–14000 cm^{-1}), windows CaF_2 (1200–8500 cm^{-1}), and a "Quartz" light source (2000–25000 cm^{-1}). In these experiments, a liquid-nitrogen-cooled InSb detector is used with an instrumental resolution of 0.01 cm^{-1}. The temperature gradient along a White cell is measured to be about 5 K between the two extremes of the multipass cell; accordingly, the average temperature is provided. In Figs. 3–7, "ap." stands for the aperture, "path" means the total pathlength of the transmitted beam, "res." stands for resolution; other parameters are clear in the notation.

In Fig. 3 *A* and *B*, we can see the partially rotational resolved v_1 H-F stretching fundamental band of the OC–HF complex near the *P*-head at 3839.12 cm^{-1}. On all

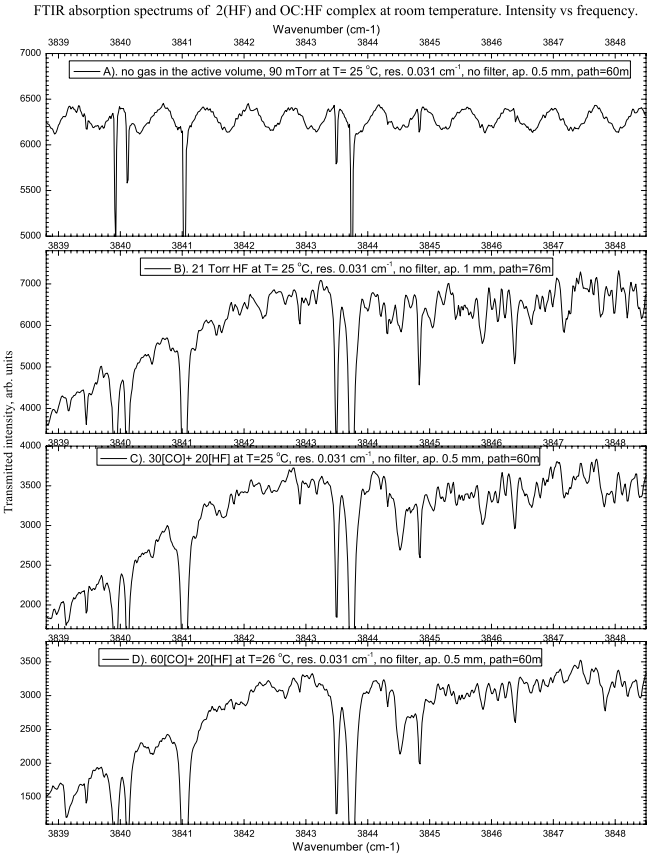

Fig. 5. Absorption spectrum of 2(HF) and OC–HF at room temperature. A is the scan of a chamber under vacuum of 90 mTorr at room temperature; B is the scan of 21 Torr of HF: 2(HF) dimer lines are overlapping with the water band of overtone lines. C and B are scans of 20 ± 1 Torr of HF with 30 ± 1 and 60 ± 1 Torr of CO, respectively

of them, the possible "P"-head of the $v_1 + v_3 - v_3$ band is visible at 3847.85 cm^{-1}.

The latter "P-head" also appears at room temperature (see Fig. 5) with twice higher CO partial pressure. Other "hot" band heads of the OC–HF complex at 3850.07 cm^{-1} and 3852.05 cm^{-1} become prominent at more higher partial pressures of the CO component at room temperature as in Fig. 6. In Fig. 6, the strong transition at 3852.1 cm^{-1} corresponds to the overtone band of water vapor. The new lines at 3850.07 cm^{-1} and 3852.05 cm^{-1} were also observed at lower temperatures and pressures, as in Fig.7.

The new lines at 3850.07 cm^{-1} and 3852.05 cm^{-1} can correspond to the second-harmonic "hot" bands $v_1 + 2v_5^0 - 2v_5^0$ and $v_1 + 2v_5^2 - 2v_5^2$ proposed as a hypothesis in [5] with regard for the appropriate anharmonicity constant describing the frequency shift 5.4076(7) cm^{-1}

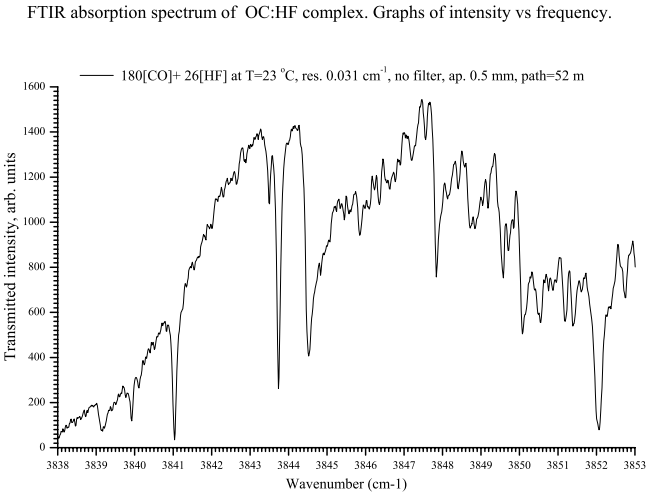

Fig. 6. Absorption spectrum of OC–HF at room temperature and a relatively high pressure of 180 Torr of the CO component

between the hot $v_1 + v_5^1 - v_5^1 = 3844.0325(3)$ cm^{-1} and fundamental $v_1 = 3849.4401(4)$ cm^{-1} bands.

In Fig. 8, we propose a reader to compare the observed spectra (shown in Fig. 3, A) with the simulated spectra based on the experimental data from Fig. 3, A) and the approximate values of the constants $B(GR) = 0.101480$ cm^{-1}; $D(GR) = 3.8 \times 10^{-7}$ cm^{-1}, $B(v_5^1) = 0.103030$ cm^{-1}; $D(v_5^1) = 3.7 \times 10^{-7}$ cm^{-1}, $B(v_3) = 0.100800$ cm^{-1}; and $D(v_3) = 3.4 \times 10^{-7}$ cm^{-1}. In the simulation, the software PGOPHER (see [46]) was used with the fixed quantities of the ground values for $v_5^1 = 81.979970$ cm^{-1} and $v_3 = 107.992200$ cm^{-1} with the Lorentzian contribution to a linewidth (full width half maximum) of 0.04 cm^{-1} and the relative line strengths (relative dipole moments – see the instruction in [46]) 1 for the transition $v_1 \leftarrow 0$, 0.85 for $v_1 + v_5^1 \leftarrow v_5^1$, and 0.7 for $v_1 + v_3 \leftarrow v_3$. The fitting (with Boltzmann weight factors) of the model linear molecule with the experimental data gave the following parameters for the excited states v_1, $v_1 + v_5^1$, and $v_1 + v_3$: $v_1 = 3844.030345$ cm^{-1} with $B(v_1) = 0.104181$ cm^{-1} and $D(v_1) = 3.447151 \times 10^{-7}$ cm^{-1}; $v_1 + v_5^1 = 3931.406563$ cm^{-1} with $B(v_1 + v_5^1) = 0.10509$ cm^{-1} and $D(v_1 + v_5^1) = 3.31263 \times 10^{-7}$ cm^{-1}; $v_1 + v_3 = 3960.72219$ cm^{-1} with $B(v_1 + v_3) = 0.102764$ cm^{-1} and $D(v_1 + v_3) = 3.059578 \times 10^{-7}$ cm^{-1}, respectively.

The state constants determined from an analysis of the fundamental v_1, hot $v_1 + v_5^1 - v_5^1$, and $v_1 + v_3 - v_3$ bands in [5] are as follows: $B(v_1) = 0.1042511(7)$ cm^{-1}; $D(v_1) = 3.040(3) \times 10^{-7}$ cm^{-1}; $B(v_1 + v_5^1) = 0.105010(11)$ cm^{-1}; $D(v_1 + v_5^1) = 3.18(5) \times 10^{-7}$ cm^{-1}; $B(v_1 + v_3) =$

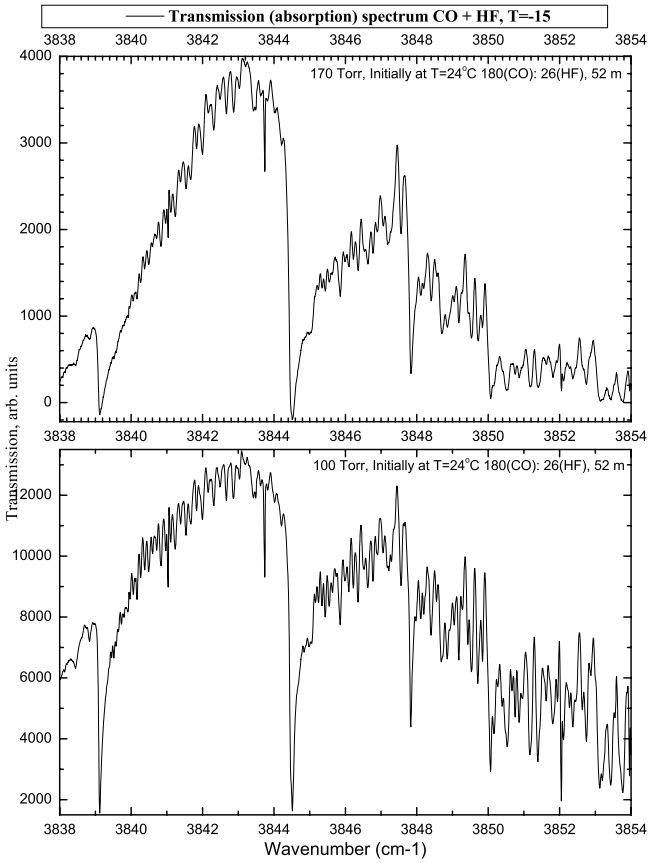

Fig. 7. Absorption spectrum of OC–HF at about -15 Celsius and relatively high pressures of the CO component with a light beam pathlength of 52 m, a filter of the interval 3750 – 3890 cm^{-1}, and an aperture of 1.5 mm. The pressure of the mixture in the lower picture was reduced manually to 100 Torr at about -15 Celsius

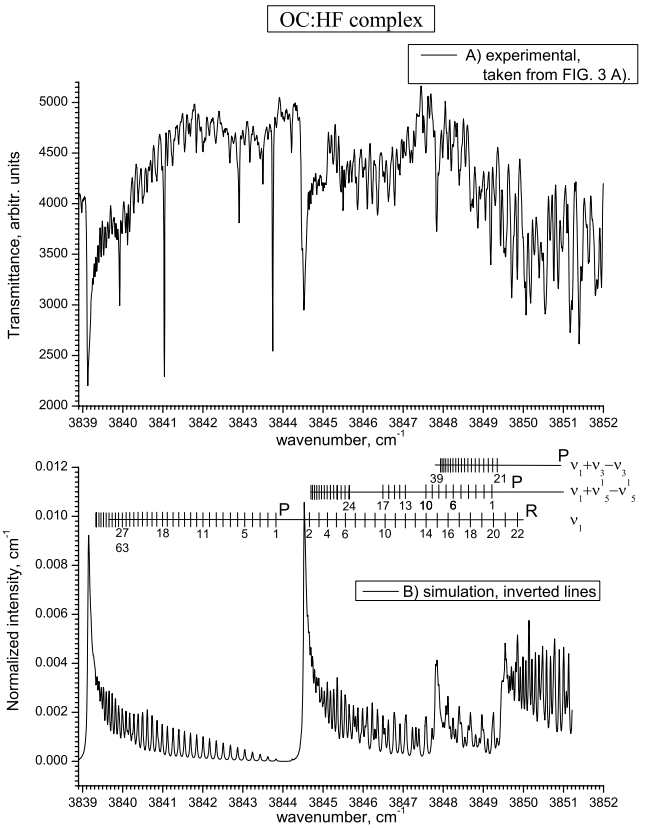

Fig. 8. The fitting (with Boltzmann weight factors) of a model linear molecule with the experimental data in Fig. 3, *A*

$0.105010(11)$ cm^{-1}; $D(v_1+v_3) = 3.18(5)\times 10^{-7}$ cm^{-1}, respectively.

The obtained spectroscopic information allows one to make a further analysis of properties of the gas phase mixture. Some thoughts and ideas of applications of the obtained data are presented in the following section.

3. Discussion of the Experimental Results

The intercomplex frequencies ν_5^1, ν_3, and ν_4^1 correspond to the temperatures 117 K (in terms of $k_\mathrm{B}T$ per the two-dimensional mode involved), 156 K (312 K in terms of $1/2k_\mathrm{B}T$ per mode), and 530 K (in terms of $k_\mathrm{B}T$ per the two-dimensional mode involved), respectively. Consequently, at the experiment temperatures from 300 K to 260 K, we can most probably observe hot bends corresponding to the frequencies ν_5^1 and ν_3. At this point, the corresponding dipole matrix elements define, which band can be more prominent. It is worth to note that the theoretical dissociation energy found in [40] by the "morphed" adiabatic potential with both monomers in their ground vibrational states is characterized by the equilibrium dissociation energy $D_e = 1310(10)$ cm^{-1} and the ground state dissociation energy $D_0 = 742.5(50)$ cm^{-1}. $D_0 = 742.5(50)$ cm^{-1}, corresponding to a quite strong binding energy with the "dissociation" temperature 1069 K (in terms of $(1/2)k_\mathrm{B}T$). In such a case, one could say that, if there is no some "barrier" to create a stable complex, potentially all monomers (for, example, HF) may exist only in bound states with the other kind of monomers (CO, accordingly). Below, we try to analyze the situation in more details.

The coupled master equation in the case of vibrational-rotational-translational exchange can be solved to find the internal state distribution in a space-homogeneous medium with one-component density number n

$$\frac{\partial}{\partial t}\rho_{iv} = \frac{n}{V}\sum_{jv'}\Big[- \rho_{iv}k\,(iv \to jv';T) +$$

$$+\rho_{jv'}k\left(jv'\to iv;T\right)\Big]; \qquad (1)$$

where ρ_{iv} are the vibrational-rotational populations with i indexing rotational states and v – vibrational ones; k is the state-to-state vibrational-rotational relaxation rate constant. The rate constants can be modeled in different ways (see, e.g., [47]). The transition rate (or, in some sense, the rate coefficient) can be expressed through the equilibrium reaction constant as $k_{\rm react}=\nu_D K_c^{\ddagger}$ with ν_D being a characteristic frequency associated with the controlling reaction coordinate. Below in this section, we discuss some possible way to define the equilibrium constant.

The used technique to compute the potential energy of the complex is essentially limited by the set of bound states with negative total energy values as, for example, in [40]. The latter does not give understanding the ways the complexes are formed. It may happen that the potential energy of a pair of monomers does not have a barrier with necessary height (see, e.g., Fig. 2), so that the tunneled "partner" monomer is caught in the potential well. In this case, the formation of dimers and higher weight complexes requires three-body collisions to "take off" the corresponding excess of translational (and vibrational-rotational) energy. Furthermore, the formation of a complex can need some rearrangement of the electronic orbits, that can use a two-step mechanism involving a virtual orbiting intermediate state stabilized by collision with the third body, so that the chemical kinetics, for instance, for molecules of one species (see [47], page 39) becomes

$$A+A\rightleftharpoons A_2^*; \qquad A+A_2^*\rightleftharpoons A_2+A; \qquad (2)$$

if the first reaction is in equilibrium, then the rate of change of the dimer number density n_{A_2} is

$$\frac{\partial}{\partial t}n_{A_2}=k_f\left[K_1 n_A^3-\frac{n_{A_2}n_A}{K_2}\right] \qquad (3)$$

with the proper equilibrium constants K_1 and K_2 and the rate constant k_f.

In addition, various collision-induced phenomena can contribute to the observed infrared absorption spectra. For example, (cited from [48]) "appreciable absorption can arise if the molecules form collision cluster, for instance if put under higher pressures, because a dipole moment is induced by the intermolecular forces. Because of the rapid decrease of intermolecular forces with increasing separation of the molecules, the induced dipole moment is a short-range function of the intermolecular distances. Consequently, the induced transition moment persists only during the time of the collision. Part of the energy of the photon which is absorbed by the collision cluster may appear as an increase in the molecular translational energy after the collision" (for all photon energy transformed into translational motion, we have pure translational transitions with $\Delta J=0$ and $\Delta m=0$ or $\Delta m\neq 0$ for the orientational transition or "flip-flop" rotational transition in the cluster with $\Delta J_1=-\Delta J_2$). The noted here especially concerns two unlike gases, when the respective electron clouds are deformed to a different degree during the collision time. In our case, both molecules (HF and CO) possess permanent dipole moment. Although the absorption, corresponding to the permanent dipole moments, gives the largest contribution to the total absorption coefficient, the simultaneous enhancement of the intensity of the dipole-allowed transitions in both kinds of monomers can happen during translational-rotational-vibrational transitions with $\Delta J_1\neq 0$ and $\Delta J_2\neq 0$, for instance. Because the observed distances between two closest "hot band" lines (in the sense of the integrated all rotational transitions in the band) are within $2\ldots 6\ {\rm cm}^{-1}$ (see Fig. 7), the pre-dissociation transitions, such like ground $\to\nu_1+\nu_{\rm rot}^{\rm monomer}$ ($\Delta j_{\rm CO}=\pm 1$), can be under consideration for the investigated mixtures.

Assuming a thermal equilibrium in the investigated gas mixtures and a quite small source intensity (a change in the upper level population has to be much less than the population value during the time corresponding to the source Rabi frequency (which is supposed to be smaller than the molecule decay rate)), one can estimate the contribution from binary and ternary collisions by investigating the dependence of the absorption coefficient (here, to stay within certain quantum optics principles, we give our edition of the expression [49] cited on the pages 415–416):

$$\alpha_{f\leftarrow i}=\frac{1}{\text{Linewidth}}\int_{Line}\alpha\left(\tilde\nu\right)d\tilde\nu=$$

$$=\frac{8\pi^3\tilde\nu_{if}g''\exp\left(-E''/k_{\rm B}T\right)\left[1-\exp\left(-h\tilde\nu_{if}/k_{\rm B}T\right)\right]}{4\pi\varepsilon_0\,3h\,c\,\delta\nu\,Q}\times$$

$$\times S_{f\leftarrow i}, \qquad (4)$$

on particle densities. Here, besides the standard constants $k_{\rm B}$, h, ε_0, and c in the IS system of units, $\tilde\nu_{if}=\frac{\left(E'-E''\right)}{h}$ is the transition frequency in Hz; g'' is the degeneracy of the level with energy E''; $\delta\nu$ is the

characteristic line width ("non-cyclic" frequency in Hz) giving the fitting of the absorption coefficient with an experimental value and may be defined by the detector characteristic time of reaction and the phase maximum frequency as for the FTIR spectroscopy using a Michelson interferometer (this was not tested with the obtained experimental results). For example, an InSb detector in our experiment has 4μs characteristic "delay" time, and the phase maximum frequency is 7899 Hz; Q is the partition function, defined as

$$Q = \sum_{\varpi} g_{\varpi} \exp\left(-E_{\varpi}/k_{\mathrm{B}}T\right), \tag{5}$$

where E_{ϖ} is the energy, and g_{ϖ} is the total degeneracy of the state ϖ. The line strength $S_{f\leftarrow i}$ of an electric dipole transition is given by

$$S_{f\leftarrow i} = \sum_{\Phi'_{\mathrm{int}},\Phi''_{\mathrm{int}}} \sum_{A=X,Y,Z} \left|\langle \Phi'_{\mathrm{int}} \left|\mu_A\right| \Phi''_{\mathrm{int}}\rangle\right|^2, \tag{6}$$

where Φ'_{int} and Φ''_{int} are eigenfunctions of the molecular Hamiltonian corresponding to the eigenvalues E' and E'', respectively; μ_A is the component of the molecular dipole moment operator along the A axis ($A = X, Y$, or Z); the (X, Y, Z) axis system has the origin at the molecular center of mass, for example, and a space-fixed orientation. The absorption coefficient per molecule can be expanded in a power series of the number density $n(SP) = N(SP)/V$ for a SP-th species ($SP = 1, 2$ for OC or HF, respectively), where $N(SP)$ is the number of SP-th molecules and V is the occupied volume:

$$\alpha^{f\leftarrow i} =$$

$$= \sum_{SP=1}^{2} \left\{ \alpha_0^{f\leftarrow i} + \alpha_{1,SP}^{f\leftarrow i} n(SP) + \alpha_{2,SP}^{f\leftarrow i} n^2(SP) + \ldots \right\}. \tag{7}$$

Here, $\alpha_0^{f\leftarrow i}$, $\alpha_1^{f\leftarrow i}$, ... are the absorption coefficients per one molecule taking binary, ternary, ... collisions into account, respectively. Because of the following use of the reviewed absorption coefficient per molecule in the expression for the transmission through the passlength z:

$$I_{\mathrm{tr}}\left(f \leftarrow i\right) = I_0\left(\tilde{\nu}\right) \exp\left[-zn\left(\mathrm{OC\text{–}HF}\right)\alpha^{f\leftarrow i}\right], \tag{8}$$

where $n\left(\mathrm{OC\text{–}HF}\right)$ is the number of complexes per unit volume, the resulting "binary" (ternary) absorption coefficient per unit passlength

$$\tilde{\alpha}^{f\leftarrow i} = n\left(\mathrm{CO\text{-}HF}\right)\alpha^{f\leftarrow i} = \tilde{\alpha}^{2,f\leftarrow i} n\left(\mathrm{CO}\right) n\left(\mathrm{HF}\right) +$$

$$+\tilde{\alpha}_1^{3,f\leftarrow i} n\left(\mathrm{CO}\right) n^2\left(\mathrm{HF}\right) + \tilde{\alpha}_2^{3,f\leftarrow i} n^2\left(\mathrm{CO}\right) n\left(\mathrm{HF}\right) + \ldots \tag{9}$$

depends on the density as the square power for binary collisions, more accurately as $n\left(\mathrm{CO}\right) n\left(\mathrm{HF}\right)$, and as the cubic number density for ternary collisions including items proportional to $n^2\left(\mathrm{CO}\right) n\left(\mathrm{HF}\right)$ and $n\left(\mathrm{CO}\right) n^2\left(\mathrm{HF}\right)$. The obtained experimental data for the transmittance can possibly answer the question: Which of the contributions from binary and ternary collisions is the most important? This, in turn, can give some picture about the possible channels of the complex creation, which was shortly described above.

For instance, assuming a quite small contribution from higher orders in densities than the 3-rd one, we calculated the three resulting absorption coefficients $\tilde{\alpha}^2$, $\tilde{\alpha}_1^3$, $\tilde{\alpha}_2^3$ in expression 9 for the intensities averaged over 18 points on the range of frequency from 3839.01 cm^{-1} to 3839.28 cm^{-1}, corresponding to the P-head of the fundamental ν_1 band. The three graphs, describing the mixture at room temperature, were chosen (Fig. 5, C and D, and Fig. 6), so that the corresponding averaged relative intensities (transmittance) are 0.045554721, 0.141861727, and 0.538861464. The latter yields the following resulting transmission coefficients: $\tilde{\alpha}^2 = 8.71 \times 10^{-51}$ m^5, $\tilde{\alpha}_1^3 = -1.26 \times 10^{-74}$ m^8, $\tilde{\alpha}_2^3 = 6.91 \times 10^{-76}$ m^8. The positive numbers potentially tells us about the main mechanism of the creation of OC–HF complexes. Therefore, the two-particle collisions of CO and HF, and the three-particle collisions CO–HF–CO are the main contributors in the complex number density. It is worth to note that the contribution from the ternary collisions CO–HF–CO is by one order lower than that from the binary ones under the provided conditions.

The concentration of the complexes $n_{00}\left(\mathrm{OC\text{–}HF}\right)$ in the ground state can be estimated using the calculated dissociation energy D_0. Assuming the main effects are due to the binary interactions as in the example above, the equilibrium reaction $A + B \rightleftharpoons AB$ can be characterized by the equilibrium constant K_{00} (see [50], Chapter 17):

$$K_{00} = \frac{n_{00}\left(\mathrm{OC\text{–}HF}\right)}{n_{00}\left(\mathrm{OC}\right) n_{00}\left(\mathrm{HF}\right)} = V \frac{Z\left(\mathrm{OC-HF}\right)}{Z\left(\mathrm{OC}\right) Z\left(\mathrm{HF}\right)} =$$

$$= \left(\frac{h^2}{2\pi\mu kT}\right)^{3/2} \frac{Z_{\mathrm{rot}}\left(\mathrm{OC\text{–}HF}\right)}{Z_{\mathrm{rot}}\left(\mathrm{OC}\right) Z_{\mathrm{rot}}\left(\mathrm{HF}\right)} \exp\left(D_0/kT\right), \tag{10}$$

where $n_{00}\left(\mathrm{OC}\right)$ and $n_{00}\left(\mathrm{HF}\right)$ are the corresponding concentrations in the ground vibrational states of the proton acceptor and the proton donor, respectively; μ is

the complex reduced mass; $Z\,(SP)$ and $Z_{\rm rot}\,(SP)$ denote the total partition function and the partition function of rotational energy levels at a certain temperature T of thermal equilibrium for a SP-th species, accordingly.

4. Conclusion

The simulated spectra and the corresponding vibrational frequencies of the OC–HF complex, described by the statistically weighted (by Boltzmann factors) transitions of the heterodimer modeled as a slightly non-rigid linear molecule (with the frequency transition expression $\nu = \nu_0 + B'J'(J'+1) - D'[J'(J'+1)]^2 - B''J''(J''+1) + D''[J''(J''+1)]^2$; here, the quantum number l is zero), are comparable with the experimental data obtained from the FTIR broadband scans of the gas phase mixtures at different total pressures and temperatures. The obtained results can be in use to make the further analysis of the gas phase properties. For example, the obtained dependence of the absorption coefficient on the partial pressures (densities) at room temperature showed the main absorption contribution from the binary collisions. Thus, the problem can be raised about the complex creation in the context of binary interactions.

The Robert A. Welch Foundation is thanked for the financial support in the form of pre-doctoral and post-doctoral fellowships under grant A-747. I also thank Dr. J. Bevan's group and the Laboratory for Submm/THz Science and Technology at Texas A & M University (College Station, Texas, USA) for providing support and consultations.

1. A.C. Legon, P.D. Soper, and W.H. Flygare, J. Chem. Phys. **74**, 4944 (1981).
2. G.T. Fraser and A.S. Pine, J. Chem. Phys. **88**, 4147 (1988).
3. J. Han, A.L. McIntosh, C.L. Hartz, and J.W. Bevan, Chem. Phys. Lett. **264**, 411 (1997).
4. Z. Wang and J.W. Bevan, J. Chem. Phys. **91**, 3335 (1989).
5. K. McMillan, D. Bender, M. Eliades, D. Danzeiser, B.A. Wofford, and J.W. Bevan, Chem. Phys. Lett. **152**, 87 (1988).
6. G.A. Jeffrey and W. Saenger, *Hydrogen Bonding in Biological Structures* (Berlin, Springer, 1991).
7. P. Hobza, in *Annual Reports on the Progress of Chemistry*, Section C, Phys. Chem. (Royal Soc. Chem., Cambridge, 2004), p. 3.
8. J.E.D. Bene and M.J.T. Jordan, Int. Rev. Phys. Chem. **18**, 119 (1999).
9. G. Gilli and P. Gilli, J. Mol. Struct. **552**, 1 (2000).
10. V.K. Pogorelyi, Russian Chem. Rev. **46**, 316 (1977).
11. G. Gilli and P. Gilli, it The Nature of the Hydrogen Bond: Outline of a Comprehensive Hydrogen Bond Theory (Oxford Univ. Press, Oxford, 2009).
12. Y. Maréchal, *The Hydrogen Bond and the Water Molecule: the Physics and Chemistry of Water, Aqueous and Bio Media* (Elsevier, Amsterdam, 2007).
13. J.C. Speakman, *The Hydrogen Bond and Other Intermolecular Forces* (Chemical Society, London, 1975).
14. P. Schuster, G. Zundel, and C. Sandorfy, *The Hydrogen Bond: Recent Developments in Theory and Experiments* (North-Holland, Amsterdam, 1976).
15. A.C. Legon, Chem. Soc. Rev. **19**, 197 (1990).
16. A.C. Legon and D.J. Millen, Chem. Rev. **86**, 635 (1986).
17. A.C. Legon, M.R. Keenan, T.K. Minton, T.J. Balle, and W.H. Flygare, J. Chem. Phys. **73**, 583 (1980).
18. E.J. Campbell, W.G. Read, and J.A. Shea, Chem. Phys. Lett. **94**, 69 (1983).
19. W.G. Read and E.J. Campbell, J. Chem. Phys. **78**, 6515 (1983).
20. Wim Klopper, Martin Quack, and Martin A. Suhm, J. Chem. Phys. **108**, 10096 (1998).
21. B. Cordero, V. Gomez, A.E. Platero-Prats, M. Reves, J. Echeverria, E. Cremades, F. Barragan, and S. Alvarez, J. Chem. Soc. Dalton Trans.**21**, 2832 (2008).
22. E.K. Kyro, P. Shoja-Chaghervand, K. Mcmillan, M. Eliades, D. Danzeiser, and J.W. Bevan, J. Chem. Phys. **79**, 78 (1983).
23. L. Oudejans and R.E. Miller, J. Chem. Phys. **113**, 4581 (2000).
24. Z.H. Yu, C.C. Chuang, P. Medley, T.A. Stone, and W. Klemperer, J. Chem. Phys. **120**, 6922 (2004).
25. I.L. Alberts, N.C. Handy, and E.D. Simandiras, Theor. Chim. Acta **74**, 415 (1988).
26. M.A. Benzel and C.E. Dykstra, J. Chem. Phys. **77**, 1602 (1982).
27. M.A. Benzel and C.E. Dykstra, Chem. Phys. **80**, 273 (1983).
28. M.A. Benzel and C.E. Dykstra, J. Chem. Phys. **78**, 4052 (1983).
29. M.A. Benzel and C.E. Dykstra, J. Chem. Phys. **80**, 3510 (1984).

30. P. Botschwina, J. Chem. Soc. Farad. **284**, 1263 (1988).

31. C. Chen, S.J. Chen, and Y.S. Hong, J. Chin. Chem. Soc.-Taip **52**, 853 (2005).

32. S.J. Chen, C. Chen, and Y.S. Hong, J. Chin. Chem. Soc.-Taip **53**, 783 (2006).

33. B. Civalleri, E. Garrone, and P. Ugliengo, J. Mol. Str. THEOCHEM **419**, 227 (1997).

34. L.A. Curtiss, D.J. Pochatko, A.E. Reed, and F. Weinhold, J. Chem. Phys. **82**, 2679 (1985).

35. A. Hinchliffe, Adv. Mol. Relax. Int. Pr. **21**, 151 (1981).

36. C.A. Parish, J.D. Augspurger, and C.E. Dykstra, J. Phys. Chem. **96**, 2069 (1992).

37. A.E. Reed, F. Weinhold, L.A. Curtiss, and D.J. Pochatko, J. Chem. Phys. **84**, 5687 (1986).

38. M.A. Spackman, J. Chem. Phys. **85**, 6587 (1986).

39. C. Tuma, A.D. Boese, and N.C. Handy, Phys. Chem. Chem. Phys. **1**, 3939 (1999).

40. L.A. Rivera-Rivera, Z. Wang, B.A. McElmurry, R.R. Lucchese, J.W. Bevan, and G. Kanschat, Chem. Phys., submitted (2011).

41. L.A. Rivera-Rivera, R.R. Lucchese, and J.W. Bevan, Chem. Phys. Lett. **460**, 352 (2008).

42. L.A. Rivera-Rivera, R.R. Lucchese, and J.W. Bevan, Phys. Chem. Chem. Phys., **12**, 7258 (2010).

43. T.S. Ho and H. Rabitz, J. Chem. Phys. **104**, 2584 (1996).

44. L. Andrews, R.T. Arlinghaus, and G.L. Johnson, J. Chem. Phys. **78**, 6347 (1983).

45. K.W. Jucks and R.E. Miller, J. Chem. Phys. **86**, 6637 (1987).

46. http://pgopher.chm.bris.ac.uk (2010).

47. David R. Miller, in *Atomic and Molecular Beam Methods*, edited by Giacinto Scoles (Oxford Univ. Press, New York, 1988), p. 38.

48. K.D. Möller and W.G. Rothschild, in *Far-Infrared Spectroscopy* (Wiley-Interscience, New York, 1971), p. 325.

49. P.R. Bunker and P. Jensen, *Molecular Symmetry and Spectroscopy* (NRC Research Press, Ottawa, 1998).

50. N.M. Laurendeau, *Statistical Thermodynamics – Fundamentals and Applications* (Cambridge Univ. Press, Cambridge, 2005).

Received 21.09.11

ФУР'Є СПЕКТРОСКОПІЯ ГАЗОВОЇ ФАЗИ CO ТА HF СУМІШЕЙ У СЕРЕДНІЙ ІНФРАЧЕРВОНІЙ ОБЛАСТІ

А.С. Сіжук

Р е з ю м е

Спектри газової фази CO та HF сумішей було досліджено за допомогою FTIR спектрометра у діапазоні частот 3838–3854 см$^{-1}$. Групи ліній комплексу OC–HF, що можуть відповідати збудженим інтермолекулярним (комплексу) розтягненням та згинам, були спостережені для парціальних тисків 20 Торр HF та 30 Торр CO і вищих. Відповідні "гарячі" групи ліній другої гармоніки моди згину були спостережені для суміші, що відповідає повному тиску 100 Торр при -15 °C (що відповідає приблизно 26 Торр HF і 90 Торр CO при кімнатній температурі). Спостережені групи ліній було визначено за допомогою моделі "слабко нетвердої" лінійної молекули. Корекція модельної лінійної молекули з експериментальними даними відтворила такі параметри для збуджених станів v_1, $v_1+v_5^1$, та v_1+v_3: $v_1 = 3844,030345$ см$^{-1}$ з $B(v_1) = 0,104181$ см$^{-1}$ і $D(v_1) = 3,447151\cdot10^{-7}$ см$^{-1}$; $v_1+v_5^1 = 3931,406563$ см$^{-1}$ з $B(v_1+v_5^1) = 0,105090$ см$^{-1}$ і $D(v_1+v_5^1) = 3,31263\cdot10^{-7}$ см$^{-1}$; $v_1+v_3 = 3960,722190$ см$^{-1}$ з $B(v_1+v_3) = 0,102764$ см$^{-1}$ і $D(v_1+v_3) = 3,059578\cdot10^{-7}$ см$^{-1}$, відповідно.

ФУРЬЕ СПЕКТРОСКОПИЯ ГАЗОВОЙ ФАЗЫ CO И HF СМЕСЕЙ В СРЕДНЕЙ ИНФРАКРАСНОЙ ОБЛАСТИ

А.С. Сижук

Р е з ю м е

Спектры газовой фазы CO и HF смесей были исследованы с помощью FTIR спектрометра в диапазоне частот 3838–3854 см$^{-1}$. Группы линий комплекса OC–HF, что могут соответствовать возбужденным интермолекулярным (комплекса) растяжениям и сгибаниям, были наблюдаемы для парциальных давлений 20 Торр HF и 30 Торр CO и выше. Соответствующие "горячие" группы линий второй гармоники моды сгибания были наблюдаемы для полной плотности смеси соответствующей давлению 100 Торр при -15 °C (что приблизительно соответствует 26 Торр HF и 90 Торр CO при комнатной температуре). Наблюдаемые группы линий были определены с помощью модели "слабо нетвердой" линейной молекулы. Коррекция модельной линейной молекулы с экспериментальными данными восстановила следующие параметры для возбужденных состояний v_1, $v_1+v_5^1$, и v_1+v_3: $v_1 = 3844,030345$ см$^{-1}$ с $B(v_1) = 0,104181$ см$^{-1}$ и $D(v_1) = 3,447151\cdot10^{-7}$ см$^{-1}$; $v_1+v_5^1 = 3931,406563$ см$^{-1}$ с $B(v_1+v_5^1) = 0,105090$ см$^{-1}$ и $D(v_1+v_5^1) = 3,31263\cdot10^{-7}$ см$^{-1}$; $v_1+v_3 = 3960,722190$ см$^{-1}$ с $B(v_1+v_3) = 0,102764$ см$^{-1}$ и $D(v_1+v_3) = 3,059578\cdot10^{-7}$ см$^{-1}$, соответственно.